

Adaptive Surface Visualization of Vessels with Animated Blood Flow

Kai Lawonn, Rocco Gasteiger and Bernhard Preim

Department of Simulation and Graphics, University of Magdeburg, Germany
{lawonn, gasteiger, preim}@isg.cs.uni-magdeburg.de

Abstract

The investigation of hemodynamic information for the assessment of cardiovascular diseases (CVDs) gained importance in recent years. Improved flow measuring modalities and computational fluid dynamics (CFD) simulations yield in reliable blood flow information. For a visual exploration of the flow information, domain experts are used to investigate the flow information combined with its enclosed vessel anatomy. Since the flow is spatially embedded in the surrounding vessel surface, occlusion problems have to be resolved. A visual reduction of the vessel surface that still provides important anatomical features is required. We accomplish this by applying an adaptive surface visualization inspired by the suggestive contour measure. Furthermore, an illustration is employed to highlight the animated pathlines and to emphasize nearby surface regions. Our approach combines several visualization techniques to improve the perception of surface shape and depth. Thereby, we ensure appropriate visibility of the embedded flow information, which can be depicted with established or advanced flow visualization techniques. We apply our approach to cerebral aneurysms and aortas with simulated and measured blood flow. An informal user feedback with nine domain experts, we confirm the advantages of our approach compared with existing methods, e.g. semi-transparent surface rendering. Additionally, we assessed the applicability and usefulness of the pathline animation with highlighting nearby surface regions.

Keywords: scientific visualization, visualization, perceptually based rendering, rendering, flow visualization, visualization

ACM CCS: I.3.3 [Computer Graphics]: Picture/Image Generation Line and curve generation

1. Introduction

The initiation and evolution of cardiovascular diseases (CVDs), such as cerebral and abdominal aneurysms, are multi-factorial problems involving hemodynamics, wall biomechanics, genetics, vessel morphology and other, not well understood, factors [AML*08]. In recent studies, domain experts identified certain hemodynamic information as important indicators for the presence, initiation and outcome of a CVD [CMWP11]; [MFK*12]. The hemodynamic information comprise quantitative measures [e.g. wall shear stress (WSS), pressure, speed] and qualitative characteristics (e.g. inflow jet, degree of vorticity), which describe the blood flow behaviour. These information are derived from patient-specific flow measuring with time-resolved phase-contrast MRI (4D PC-MRI) [MFK*12] or computational fluid dynamics (CFD) simulations [CCA*05]; [KBDL09]. Furthermore, for particular CVDs, such as cerebral aneurysms, CFD simulations provide clinically relevant information regarding treatment options by conducting virtual treatments [AML*08]. The acquired hemodynamic information are

very complex because they consist of several multivariate (e.g. scalar and vector data) and multi-dimensional (3D and 4D) information. In addition to a quantitative analysis, an effective visual exploration of these attributes is important to obtain insights based on this information. For the visual exploration, domain experts, such as biomedical researchers and CFD blood flow experts, are interested in the hemodynamics *and* the surrounding vessel anatomy because both information are strongly correlated to each other [BSH*10]. On the one hand, this leads to an embedded surface problem where the flow is occluded by the surrounding vessel surface. These occlusions have to be resolved in such a way that important anatomical surface features are still depicted, while simultaneous visibility of the embedded flow visualization is ensured. On the other hand, the dynamic behaviour of the time-dependent flow data sets have to be conveyed, especially the correlation between near-wall flow patterns and surface features. It is assumed that abnormal near-wall flow leads to pathological vessel dilatations and may increase the risk of a new rupture at locations where a former rupture occurred. Existing techniques, such as semi-transparent rendering or clipping

of the vessel surface, exhibit a reduced surface shape depiction and ambiguities of the spatial relationship between vessel sections. This decreases the observers' ability to mentally link the vessel morphology with the internal flow visualization. Gasteiger *et al.* [GNKP10] tackled this embedded surface problem and proposed an adaptive surface visualization that incorporates a ghosted view approach. The ghosted view leads to a completely occluded flow visualization below surface regions that are facing away from the viewer. Furthermore, the view-dependent opacity does not ensure an appropriate depiction of salient concave and convex surface regions, which are necessary to identify pathological bulge formations of the vessel wall. Inspired by illustrative line rendering techniques, we propose an adaptive surface rendering that overcomes these limitations. In a recent comparison of feature line approaches, the *suggestive contours* technique exhibits the most effective shape description for patient-specific anatomical surfaces [LGP13b]. Therefore, we developed a surface shading that incorporates the view-dependent curvature of suggestive contours into the ghosted view approach of Gasteiger *et al.* [GNKP10]. This ensures the visibility of the embedded flow visualization and the expressive depiction of salient vessel surface features as well as highlighting nearby surface regions from animated pathlines. In summary, the contributions of this paper are:

- We present a novel technique for vessel visualization with embedded blood flow information, depicted with established flow visualization methods that is an extended version of a previous paper [LGP13a].
- We derive our method from an established feature line technique—*suggestive contours*.
- We demonstrate that our method is applicable to arbitrary vessel surfaces, but also to other patient-specific anatomy.
- We introduce an animated pathline approach where nearby surface regions are highlighted to gain spatial information of the interior blood flow.

2. Medical Background and Requirement Analysis

CVDs refer to the class of diseases that effect the heart and blood flow vessels (arteries and veins). Common examples of CVDs are aortic aneurysms and dissections, cerebral aneurysms or atherosclerosis. For the identification, progression and risk assessment of CVDs, the blood flow behaviour plays an important role. A particular example are cerebral aneurysms, which are pathological dilations of the vessel wall that exhibit an increased risk of rupture [Juv11]. Risk factors and other relevant flow characteristics are identified by quantitative and qualitative analyses. We focus on the qualitative analysis, which involves a visual exploration of the morphology *and* its embedded blood flow information. Domain experts require the visualization of both information because they strongly influence each other. For example, in the case of cerebral aneurysms, a bleb formation indicates a previous rupture and increases the risk of further ruptures. Blebs are local bulges on the aneurysm sac and can be found at regions of high WSS and near the flow impingement zone. Thus, an expressive surface depiction that conveys such morphological features but ensures both visibility of the underlying flow and indication near-wall flow is necessary.

2.1. Requirement analysis

A detailed visual description of the enclosing vessel surface leads to an increased occlusion of internal information. Thus, an adapted surface visualization is needed to reduce the occlusion. Based on literature and discussions with domain experts, we address the following requirements:

2.1.1. Visibility of internal flow information

A maximum visibility of the internal flow visualization is required during the visual exploration. With 'maximum visibility', we mean as few as possible occlusions of the flow visualization by means of the enclosing surface. This supports the viewer in interpreting and tracing the flow.

2.1.2. Emphasis of relevant surface features

As vessel morphology and flow influence each other, an expressive vessel shape depiction is necessary that conveys surface features such as concave and convex regions as well as bleb formations.

2.1.3. Revealing pathline-nearby surface information

Since hemodynamic information, e.g. speed, pressure and vorticity, is important for blood flow assessment, an animated pathline animation has to be provided. To improve the perception of the position of the animated pathlines, a highlighting of nearby surface regions is favourable.

2.1.4. Improvement of depth perception

For the depiction of overlapping and distant vessel parts, depth cues should be provided. These hints improve the perception of depth and spatial relationships of the vessel surface and attract the attention to vessel regions that are close to the viewer.

3. Related Work

Effective embedded surface visualizations are relevant in several domains like engineering, vector field analysis, medical research and treatment planning. Each scenario is faced with occlusions and challenges regarding perception of shape, depth and spatial relationship. Thus, several visualization domains are involved to cope with these challenges.

3.1. Illustrative shape visualization

Illustrative shape visualizations aim at reproducing artistic drawings to convey surface shape details by means of shading, texturing and pen-and-ink techniques [SABS94]. Existing approaches are mainly based on local geometry and illumination information such as normals, curvature measures and changes of luminances. Examples of non-photorealistic shading models, which focus on surface shape enhancement, are proposed by Gooch *et al.* [GGSC98] and Rusinkiewicz *et al.* [RBD06]. Fundamental questions concerning shape perception based on texture patterns were investigated by

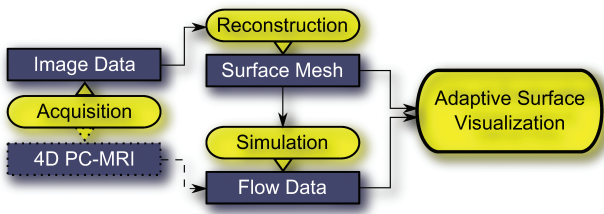


Figure 1: Data acquisition pipeline to obtain the vessel surface and blood flow information for our approach.

Kim *et al.* [KHSI04]. While all of these shading- and texture-based approaches enhance surface shape, they rely on an opaque surface rendering, which is not applicable for enclosing vessel surface rendering. However, we incorporate information about the local normal orientation to convey local surface orientation such as concave and convex regions. A reduced 3D surface description can also be accomplished by illustrative line renderings such as *silhouettes* [IFH*03] and other features lines. Interrante *et al.* [IFP95] proposed *ridge and valley lines*, which are defined as the loci of points at which the principle curvature reaches an extremum in the principle direction. DeCarlo *et al.* [DFRS03] developed *suggestive contours* that are defined as the set of minima of the diffuse headlight in view direction. *Apparent ridges* were introduced by Judd *et al.* [JDA07] who extend the ridge and valley lines by using view-dependent curvature direction. Xie *et al.* [XHT*07] presented *photic extremum lines* (PELs) defined as the loci of points where the variation of illumination in its gradient direction reaches a local maximum. In an informal evaluation, Lawonn *et al.* [LGP13b] figured out that suggestive contours provide the most visually pleasing results on patient-specific anatomic data sets. Depending on the flow visualization technique, the generated lines and stripes on the surface may cause visual clutter in a combined visualization, e.g. in case of integral lines as flow visualization technique. Thus, we only consider silhouettes as suitable for our application.

3.2. Visualization of embedded structures

Interrante *et al.* [IFP97] investigated how sparsely-distributed opaque texturing can be used to depict the shape of transparent iso-intensity surfaces of radiation dose as a special instance of an embedded surface visualization problem. An interactive view-dependent transparency model was proposed by Diepstraten *et al.* [DWE03] to improve the shape perception of embedded structures. Based on several *design rules*, the transparency and visibility of the layered objects are adjusted according to the camera view and the spatial relationship between opaque and semi-transparent objects. This kind of visualization is an example of ghosted views and belongs to the group of *smart visibility techniques*. These techniques focus on exposing the most important visual information and originate from technical illustration. Other examples are cut-away views, section views and exploded views [Vio05]. A multi-pass framework for illustrative rendering of complex and self-occluded integral surfaces was proposed by Hummel *et al.* [HGH*10] and Born *et al.* [BWF*10]. They incorporated several rendering techniques, such as transparency modu-

lations, hatching textures, halftoning and illustrative streamlines, to reveal subjacent layers and to enhance shape and depth perception of each layer. In Gasteiger *et al.* [GNKP10], a multi-pass framework was presented that incorporates some of the design rules of Diepstraten *et al.* [DWE03] to achieve a ghosted view for enclosing vessel surfaces with embedded flow information. The opacity of the vessel surface is controlled by a Fresnel opacity term. Baer *et al.* [BGCP11] confirmed the performance of the visualization in a quantitative user study. However, a limitation of the ghosted view method becomes obvious in regions that are oriented away from the viewer and occlude the underlying flow visualization. Additionally, salient surface regions described by concave and convex regions may not be well conveyed by the Fresnel opacity.

3.3. Illustrative flow visualization

For an extensive overview of flow visualization, we refer to the state-of-the-art surveys by McLoughlin *et al.* [MLP*10] (geometric-based), Salzbrunn *et al.* [SJWS08] (partition-based) and Laramee *et al.* [LHZP07] (topology-based). In Mattausch *et al.* [MTHG03] and Everts *et al.* [EBR*11] illustrative line style methods, such as halos, glyphs and depth attenuations, were utilized to enhance the perception of dense streamline and pathline data sets. Van Pelt [Pel12] presented real-time illustrative visualization and exploration methods for measured cardiac blood flow. Born *et al.* [BMGS13] and Köhler *et al.* [KGP*13] introduced approaches for the extraction and illustrative depiction of flow structures in measured blood flow based on the concept of line predicates. Gasteiger *et al.* [GNBP11] introduced the *FlowLens*, an interactive focus-and-context tool for the exploration of multiple flow attributes for simulated and measured blood flow. For example, the animation of pathlines could be observed within the lens and relevant context attributes, such as WSS and pressure, outside the lens. A system for the qualitative exploration of near-wall hemodynamics in cerebral aneurysms was presented by Neugebauer *et al.* [NLB*13]. A recent overview about visual exploration methods and future visualization challenges for simulated and measured flow data sets are given by Preim and Botha [PB13] and Vilanova *et al.* [VPvP*12], respectively.

3.4. Conveying depth and spatial relationship

Our application is also related to perception-based 3D graphics. Two important cues for depth and spatial arrangement are shadowing and shading [WFG92]. In Luft *et al.* [LCD06], an image-based method was presented to efficiently integrate depth cues into complex scenes based on the differences between the depth buffer and its low-pass filtered copy.

Further depth cues are atmospheric attenuation, depth blurring and line fading, which are discussed in Svakhine *et al.* [SEA09]. The shadow approximation proposed by Luft *et al.* [LCD06] and atmospheric attenuation were also utilized by Gasteiger *et al.* [GNKP10] to enhance the depth perception of vessel regions. Shadow-like depth indicators by means of an adaptive hatching method were proposed by Ritter *et al.* [RHD*06] to support reliable comparisons of spatial distances in complex vascular structures. A weighted combination of illustrative rendering techniques was utilized by Tietjen

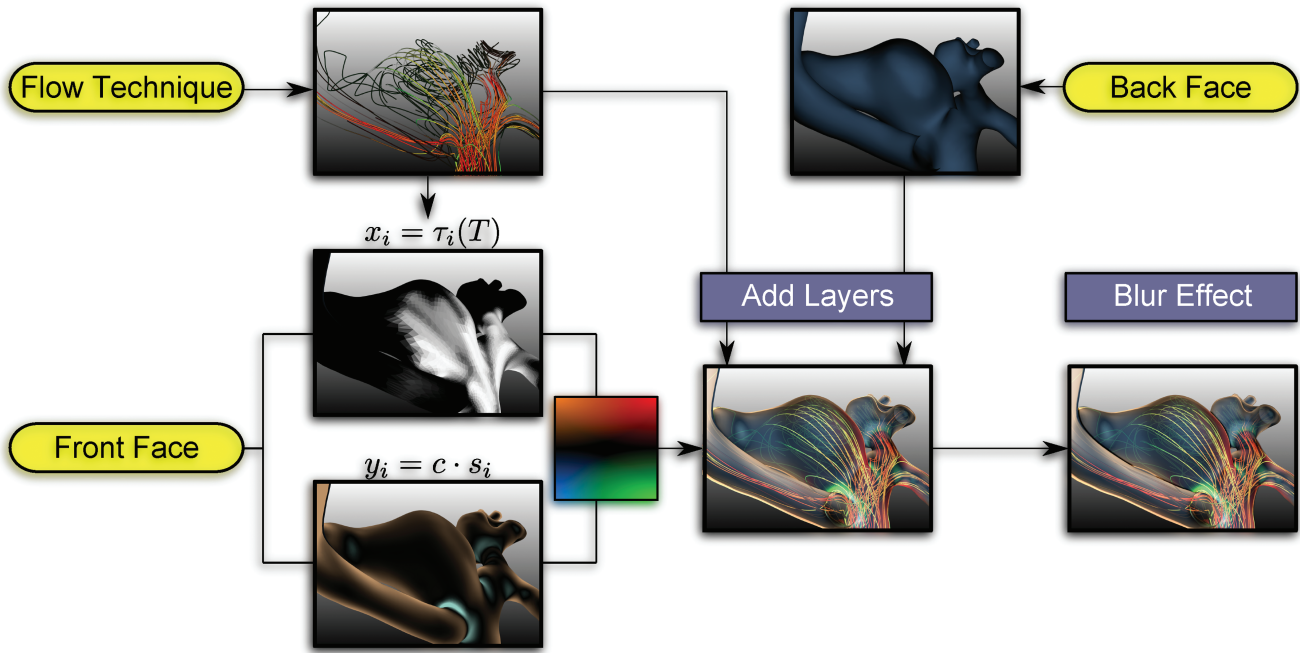


Figure 2: Overview of our adaptive surface visualization: Firstly, we visualize the blood flow with established flow visualization techniques, e.g. pathlines. Secondly, we determine the shading of the front faces. This calculation is based on the (x, y) coordinates. For the x coordinate, we use distances of the pathlines to the surface. The y coordinate is determined according to the suggestive contour measure. The back faces are rendered opaque. Finally, we compose each visualization layer and add shadow approximation as well as depth blurring to the result.

et al. [TPB*08] for depth- and shape-enhanced medical surface visualizations inspired by medical textbook illustrations. The weighting is controlled by a *shading map*, which combines several illumination and surface information such as plateau and raking light, atmospheric attenuation and curvature.

4. Data Acquisition Pipeline

Before we present the details of our method, we briefly describe the steps to generate the needed vascular surface and blood flow data. The data acquisition pipeline consists of three steps, illustrated in Figure 1.

4.1. Acquisition

In the first step, clinical image data (CTA, MRA, 3D rotational angiography) of the vessel are acquired. If 4D PC-MRI (phase-contrast MRI) is available, a full 3D flow measuring over time can be performed, which encodes the flow direction and magnitude at each voxel [MFK*12]. Measuring errors introduced by eddy currents, noise and velocity phase wraps are reduced according to several filter methods described in Hennemuth et al. [HFS*11].

4.2. Surface reconstruction

In the second step, the vessel surface is reconstructed based on a vessel segmentation. Because of the high vessel-to-tissue contrast in the image data, often a simple thresholding segmentation followed

by a connected component analysis is sufficient to separate the vessel from the surrounding tissue. Artifacts resulting from image acquisition and contrast agent distribution can erroneously merge adjacent branches or lead to erroneous narrowings. They need to be manually corrected, see [MNP11] for a description of this process. More advanced techniques like active shape models and deformable models can be employed to minimize the manual effort in cases of low intensity distribution [LABFL09]. The resulting segmentation mask is used to reconstruct the surface with marching cubes and optimized with respect to mesh quality by a combination of edge collapses and edge flips [Sch97].

4.3. Simulation

The optimized surface mesh is utilized for generating an unstructured volume mesh, as an input for the subsequent CFD simulation. In most cases, the blood is modelled as Newtonian fluid with steady or unsteady flow and rigid walls. Cebra et al. [CCA*05] have shown that with these assumptions a qualitative flow characterization is still possible.

5. Method

The presented method for the novel adaptive surface visualization is based on the multi-pass framework proposed by Gasteiger et al. [GNKP10] and incorporates different visualization techniques, as illustrated in Figure 2. We improve the ghosted view approach by modifying the vessel opacity of the front faces by means of the

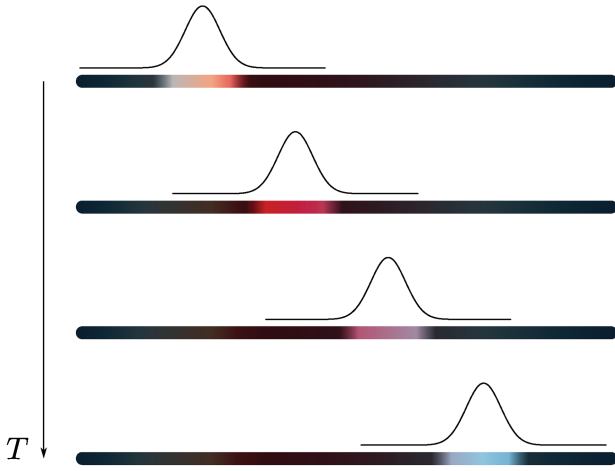


Figure 3: A pathline with additional colour-coded information is illustrated. During the animation a Gaussian distribution runs over the pathline to highlight corresponding parts.

suggestive contour measure. Furthermore, we utilize depth blurring instead of atmospheric attenuation because of the more natural depth perception. We first recap the suggestive contours technique and present its incorporation into our modified ghosted view shading approach afterwards.

5.1. Suggestive contours

We briefly explain how *suggestive contours* are determined. *Suggestive contours* are view-dependent feature lines based on second order derivatives. These lines are defined as the set of minima of $\mathbf{n} \cdot \mathbf{v}$ in the direction of \mathbf{w} , where \mathbf{n} is the unit surface normal, \mathbf{v} is the view vector (which points to the camera) and \mathbf{w} is the projection of the view vector on the tangent plane. Precisely:

$$D_{\mathbf{w}}(\mathbf{n} \cdot \mathbf{v}) = 0, \text{ and } D_{\mathbf{w}}D_{\mathbf{w}}(\mathbf{n} \cdot \mathbf{v}) > 0,$$

where $D_{\mathbf{w}}(\mathbf{n} \cdot \mathbf{v})$ denotes the derivative of the scalar value $\mathbf{n} \cdot \mathbf{v}$ in the direction of the vector \mathbf{w} . First, one has to evaluate $\mathbf{n} \cdot \mathbf{v}$ per vertex. Afterwards, the gradient $\nabla(\mathbf{n} \cdot \mathbf{v})$ is determined for each triangle $t = (\mathbf{p}_1, \mathbf{p}_2, \mathbf{p}_3)$. Every vertex $\mathbf{p}_1, \mathbf{p}_2, \mathbf{p}_3$ obtains a scalar value. These values are calculated by the dot product of the associated vertex normal \mathbf{n}_j , $j \in \{1, 2, 3\}$ and the view vector \mathbf{v} : $l_j = \langle \mathbf{n}_j, \mathbf{v} \rangle$. The light gradient ∇l of the triangle $t = (\mathbf{p}_1, \mathbf{p}_2, \mathbf{p}_3)$ is determined by:

$$\nabla l_{\Delta} = (l_2 - l_1) \frac{(\mathbf{p}_1 - \mathbf{p}_3)^{\perp}}{2A_{\Delta}} + (l_3 - l_1) \frac{(\mathbf{p}_2 - \mathbf{p}_1)^{\perp}}{2A_{\Delta}}, \quad (1)$$

where A_{Δ} denotes the area of the triangle and \perp stands for a counterclockwise rotation by 90° in the triangle plane, see [BKP*10]. Next, we use the triangle gradient to determine the vertex gradient. For this purpose, we consider the adjacent triangles of a vertex and rotate each face gradient into the vertex's tangent space. After-

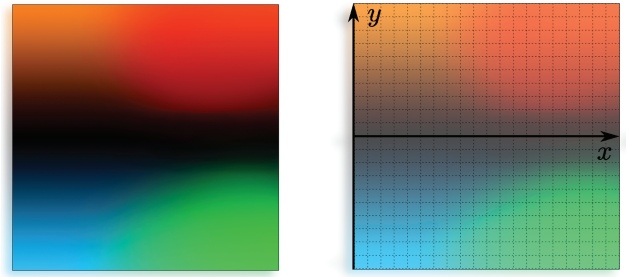


Figure 4: The 2D texture lookup table (LUT) and its coordinate system that represents the colour coding for concave (cyan) and convex (orange) as well as pathline-near (red) and pathline-far (green) vessel surface regions.

wards, we average the gradients according to their voronoi area, as described by Meyer *et al.* [MDSB02], and obtain the light gradient $\nabla l_i = \nabla(\mathbf{n}_i \cdot \mathbf{v})$ for the i th vertex. Finally, given the view vector \mathbf{v} , the light gradient ∇l_i , and the corresponding normalized vertex normal \mathbf{n}_i , we project \mathbf{v} onto the tangent space of the i th vertex. So, we get $\mathbf{w}_i = \mathbf{v} - \mathbf{n}_i \mathbf{n}_i^T \cdot \mathbf{v}$. The feature lines are defined as the zero-crossing of the dot product $\mathbf{w}_i \cdot \nabla l_i$ by linearization in the interior of a triangle. Furthermore, lines are drawn if the derivative magnitude is larger than a user-defined threshold. However, objects without concave regions have no *suggestive contours*.

5.2. Pathline animation

Domain experts are also interested in the dynamic behaviour of the time-dependent flow characteristics. Therefore, we extracted pathlines out of the flow data sets with an adaptive Runge-Kutta scheme [TGE97]. To support the blood flow assessment, we animate the pathlines over time to convey speed information. However, the whole pathline is visualized and colour-coded with additional information, such as curvature or vorticity, as context information. For avoiding visual clutter, we use desaturated colours and enhance parts of the pathlines with a Gaussian distribution during the animation, see Figure 3. In addition, we have given a scalar field $t(\mathbf{q})$ as time information for each individual pathline. This scalar field represents the pathline point \mathbf{q} in time where the pathline passes the corresponding surface location. For example, having the time $t(\mathbf{q})$ at point \mathbf{q} means that the pathline passes \mathbf{q} at that time $t(\mathbf{q})$. In detail, we use the distribution for the animation of a single pathline:

$$f(T, \mathbf{q}) = \alpha \cdot e^{-\frac{(T-t(\mathbf{q}))^2}{\beta}},$$

where T denotes the animation time. Therefore, each pathline PL has a maximal time length $t'(PL)$. As the points of the pathline $\mathbf{q}_i \in PL$ with $i \in \{0, \dots, N\}$ are consecutively ordered it yields $t'(PL) = t(\mathbf{q}_N)$. For the animation, the value T runs from 0 to the maximal time value $\max_{PL} t'(PL)$.

For α , we set $\alpha = 1$ because we want to illustrate the original colour of the pathline at \mathbf{q} with $T = t(\mathbf{q})$. The parameter β

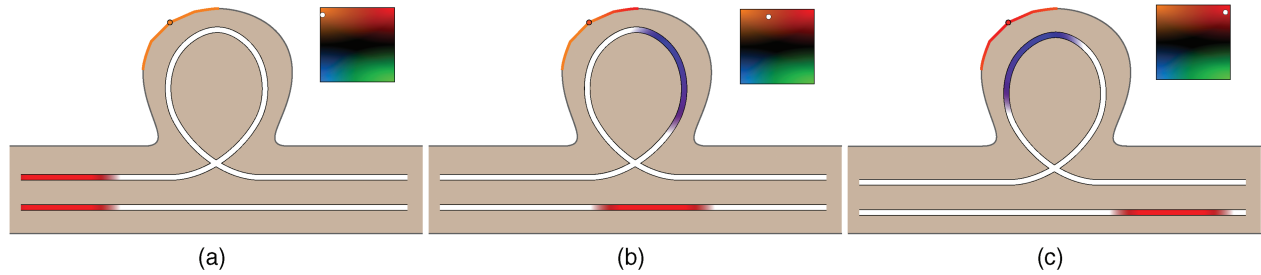


Figure 5: A schematic view of our approach. First, every point is assigned to (x, y) coordinates of the LUT. In (a) to (c) the x coordinate changes because the highlighted pathline gets closer to the point on the surface. In (c), the pathline is closest to the point and therefore obtains the colour red. Note that in this example the viewpoint is always the same and therefore no change of the y coordinate occurs.

represents the length of highlighted parts on the pathline. The smaller β , the smaller the highlighted part. We suggest to determine β by computing the median (med) of the animation times $t'(PL)$ of all pathlines: $med_{PLt'}(PL)$. Finally, we set $\beta = 2 \cdot med_{PLt'}(PL)$ as default value, but the user can adjust it during runtime.

The highlighting function f is multiplied with the colour coding of the pathlines. To avoid rather dark areas, f is clamped to the interval $[0.25, 1]$. Therefore, the pathlines are still perceivable even if the animation at the current time point does not result in a highlighting of a pathline. Furthermore, we choose the highlighting function f as to be time-dependent regarding the integration time. Thus, having a pathline that runs faster through the vessel than the other, the highlighted parts are wider. This supports the perception of fast pathlines and is based on the idea of a trail that is longer when the object is faster.

5.3. Highlighted surface regions

To improve the visual exploration of the animated pathlines, we employ an enhanced illustration of the pathline-nearby surface region. Therefore, we determine a time-dependent scalar field $\varphi(\mathbf{p}, T)$ on the surface mesh. This scalar field contains the minimal distance of all highlighted pathline parts regarding the animation time T . Thus, $\varphi(\mathbf{p}, T)$ encodes the minimal distance from surface point \mathbf{p} at time T to a highlighted pathline part.

Next, we transform this scalar field such that surface parts distant to highlighted pathline parts are assigned to zero, whereas nearby regions are at most 1. We will explain this choice in Subsection 5.4. We transform the scalar field by:

$$\tau(\mathbf{p}, T) = 1 - \frac{1}{\gamma} \cdot \varphi(\mathbf{p}, T).$$

For the surface mesh, we write $\tau_i(T) := \tau(\mathbf{p}_i, T)$ to indicate the position of the vertex. The parameter γ can be seen as a threshold for distances. We determine γ by calculating the 1% quantile, namely percentile. Therefore, we set γ as the 1% quantile of the set of distances ordered from low to high. This ensures that τ is higher than zero for values less than the 1% quantile and less than for values higher than the 1% quantile.

5.4. Feature regions

Our shading is defined by two values and a lookup table (LUT), see Figure 4. The first value per vertex is given by

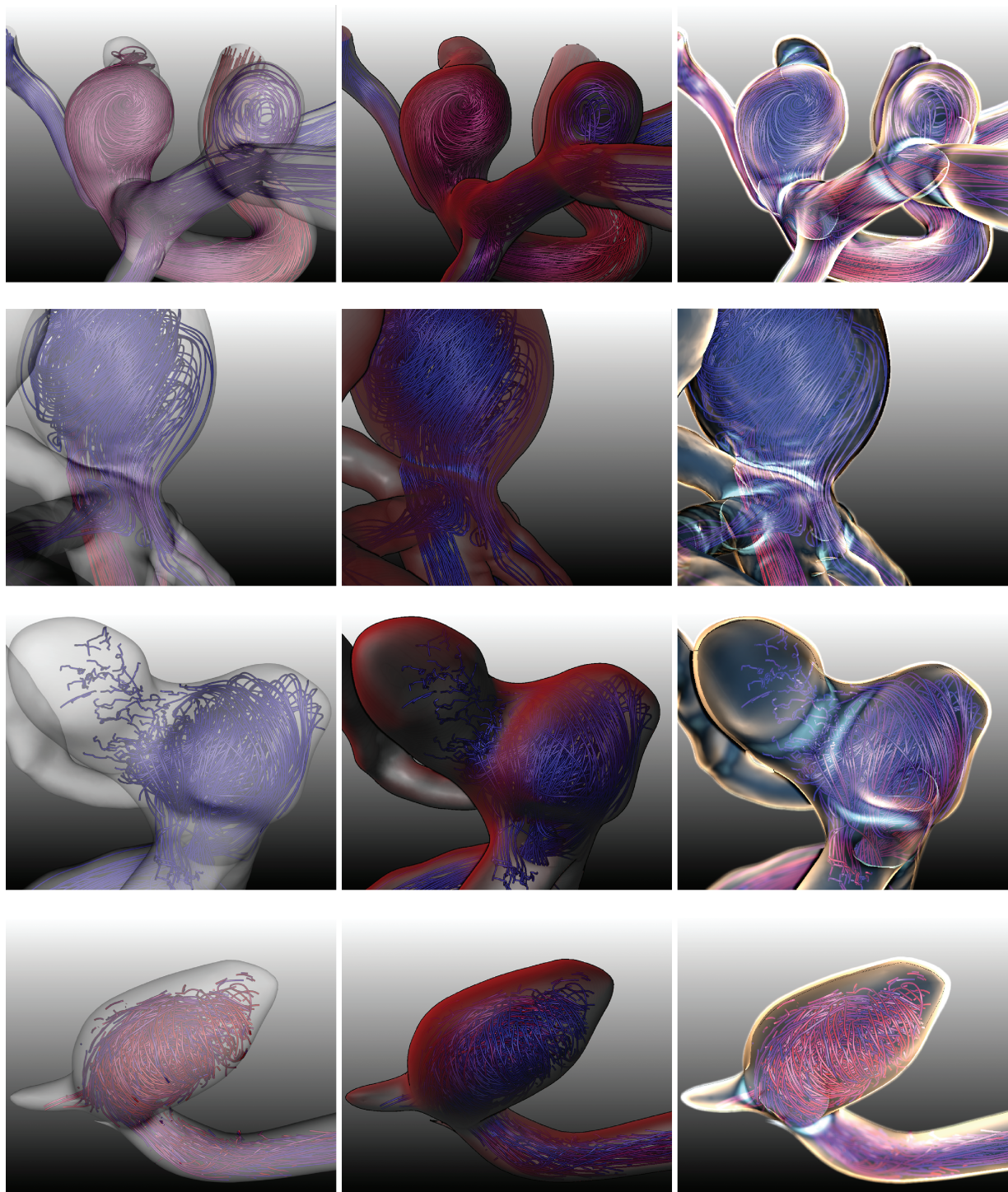
$$y_i = c \cdot s_i = c \cdot (\mathbf{w}_i \cdot \nabla l_i)$$

with the values defined in Section 5.1. Here, c is a user-defined value, which adjusts the brightness of the shading. Prominent highlights are defined as zero-crossings of s_i and we convey these regions with an expressive colour coding. Thereby, we differentiate between negative and positive values of s_i . The second value per vertex is given by

$$x_i = \tau_i(T) = 1 - \frac{1}{\gamma} \cdot \varphi(\mathbf{p}_i, T)$$

with the values defined in Section 5.3. The assignment of the colours for each vertex is performed by a 2D LUT. We use the values (x_i, y_i) to assign the defined colour to vertex i . This is defined by the RGB value position (x_i, y_i) in the LUT. The LUT has coordinates $[0, 1] \times [-1, 1]$ and therefore we clamp (x_i, y_i) to $[0, 1] \times [-1, 1]$ as well. Figure 5 shows an example of the colour LUT application during the animation.

To differentiate the regions, we choose two antipodal colours in the CIELab colourspace. First, we choose a colour $col_1 = \{L, a, b\}$, in our case orange with $col_1 = \{65, 51, 74\}$, and change the signs of a, b . So, we get $col_2 = \{L, -a, -b\}$, in our case $col_2 = \{65, -51, -74\}$, cyan. Thus, we obtain two different coloured regions where the border represents a feature derived by *suggestive contours*. These colours are used for the y -axis of the LUT. Orange represents the positive y values and cyan the negative ones. Both colours have a linear colour gradient from black at $y = 0$ to $y = 1$ orange and accordingly to $y = -1$ cyan. For the x -axis, we decrease the H value from the HLS colour space such that we obtain red for $(1, 1)$ and green for $(1, -1)$. In summary, we obtain a LUT with $(x, 0) \triangleq$ black, $(0, 1) \triangleq$ orange, $(0, -1) \triangleq$ cyan, $(1, 1) \triangleq$ red and $(1, -1) \triangleq$ green. The transitions of the colours are linear. Additionally, we determine the colour on the surface mesh and compose it with the backface surface colour. The result is a shading, which conveys the impression of a Fresnel opacity with highlighted surface features.



Semitransparency

Fresnel opacity [GNKP10]

Our shading

Figure 6: *Our shading in comparison with semi-transparent visualization and Fresnel opacity [GNKP10] for different vessels with internal flow depicted with illustrative streamlines. The semi-transparent approach fails to give a spatial impression. The Fresnel opacity approach provides good visual results, but some streamlines are occluded by fully opaque vessel regions facing away from the viewer. Our approach overcomes these limitations and the streamlines are depicted well.*

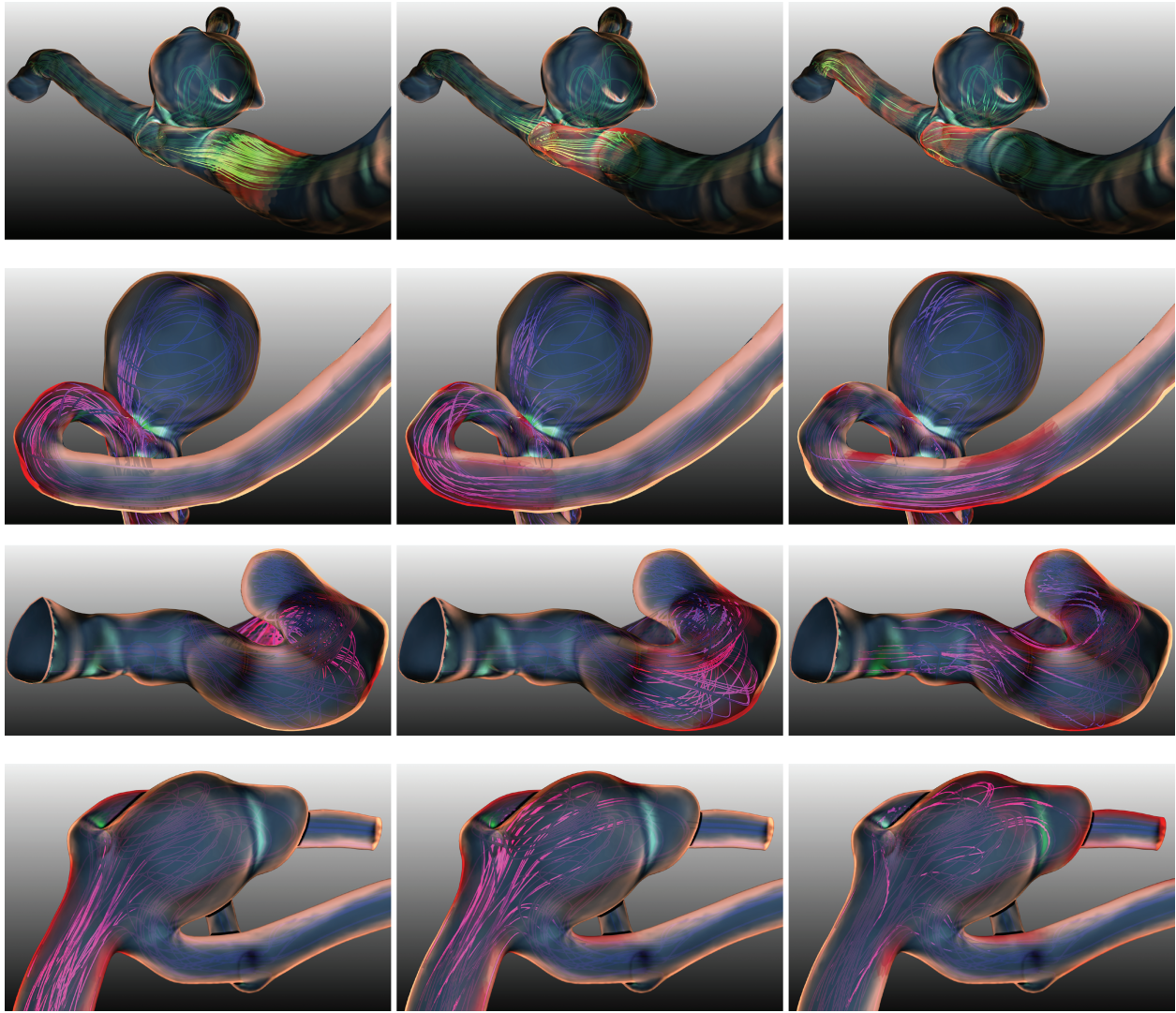


Figure 7: Our adaptive surface approach highlights pathline-nearby surface features during the animation of the pathlines. In the first row, we used a different colour-coding for the pathlines than for the other data sets.

5.5. Visual effects

We added some visual effects to emphasize the region of interest. First, we apply an approximated shadow casting onto the front faces of the vessel surface to enhance the spatial relationship between overlapping vessel sections. Here, we implemented the method proposed by Luft *et al.* [LCD06] and compute a *spatial importance function* from the depth buffer and its low-pass filtered version. The low-pass filtering is accomplished by a Gaussian blurring and the result is subtracted from the original depth buffer. Negative values represent areas of background objects that are close to other occluding objects. The shadow casting is approximated by adding the negative values to the original colour values, which causes a local darkening.

Furthermore, we consider a focus region as basis for focus-and-context visualization as well as depth attenuation. This region is defined by a depth-near and depth-far region adjusted by the user.

Thus, pathological regions, such as the aneurysm sac or a stenosis, can be emphasized. Vessel sections, which are outside this region, will be blurred according to a Gaussian blurring filter with a kernel size that linearly depends on the distance between vessel sections and the focus region. This leads to a smooth transition between the focus region and the surrounding that supports both attraction to the focus region and perception of depth. The blurred vessel sections with their embedded flow visualization are still provided as context information (see Figure 2, right).

6. Algorithm and Implementation

The algorithm of our shading comprises the following steps:

1. (Optional) Subdivide and smooth the mesh.
2. Determine distances of the surface to the pathlines.

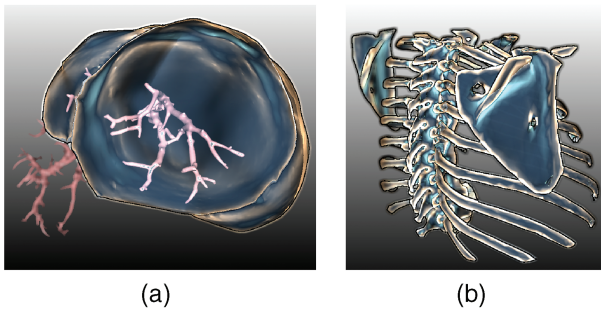


Figure 8: Our adaptive surface approach can also be applied to non-vessel surfaces such as (a) liver surfaces with portal vein and (b) bone structures.

3. Compute vertex normals.
4. Build neighbour information.
5. Determine vertex gradients.
6. Compute colour for each vertex.
7. Blur the rendered image and add shadows.

The algorithm is divided in two parts. The first part (1–4) consists of several preprocessing steps and the second part (5–7) is the rendering loop. Both are described in more detail in the following sections.

6.1. Preprocessing

At the beginning, we determine the time-dependent scalar field on the surface mesh that encodes the distances of the pathlines. For every vertex, we measure the distances to the pathline points and chose the shortest one for each time step. Therefore, we obtain several scalar values for each vertex, which encode the distances for every time step. We store the values by using a rectangle texture `GL_TEXTURE_BUFFER`. This texture has size $\#vertices \times \#timesteps$ and stores the values of x_i , as described in Section 5.3. The determination of the minimal distances is computationally intensive. As this computation is a preprocessing step, we simply compare the distances for each vertex and each point on the pathlines. An improvement of this method would be to use k-d trees [Ben75] and adapt them to the GPU [ZHWG08].

After the computation of the time-dependent scalar field, we compute the vertex normals by averaging the area-weighted normals over adjacent faces. For the neighbourhood information of a vertex, we use the OpenGL extension `GL_ARB_SHADER_STORAGE_BUFFER_OBJECT`, which is part of the OpenGL core since version 4.3. With this, we create a three-dimensional integer vector. The first component consists of the ordered neighbours of the vertices. The second component stores the number of neighbours in the associated list entry. In the third component, we write the offset index where we can find the entry for the first component.

6.2. Rendering loop

During runtime, steps 5, 6 and 7 are executed in a two-pass rendering. In the first pass, we determine the vertex gradient in the vertex shader, which depends on the camera and the light position. Subsequently, we compute and assign the pixel colour in the fragment shader as described in Sections 5.3 and 5.4. In the second pass, we apply the Gaussian blurring and shadowing as presented in Section 5.5.

During the pathline animation, the user is able to adjust typical animation settings such as: play, stop, next frame, previous frame, slower and faster. The animation stops if the user rotates the scene to avoid visual distractions during the exploration. Therefore, the user can adjust the camera for a better view and the animation continues afterwards.

6.3. Interface

For the visual exploration of the pathlines, a graphical user interface must be provided. For this, we employ buttons in the style of standard media players. This includes a *play*, *pause*, *forward* and *backward* button. Furthermore, a timeline is provided. The play button starts the animation, whereas the pause button stops the animation, but the current frame step is kept. The forward and backward buttons are useful to guide the animation step by step. Additionally, we provide the possibility to jump to a certain keyframe by clicking on the corresponding position on the timeline. This ensures an intuitive and fast exploration of the animation.

7. Evaluation

This section is divided into two parts. In the first part, we examine our surface shading in comparison to other methods. We conducted an evaluation to assess the possibility to perceive surface information as well as flow data. In the second part, we evaluated the pathline animation as well as the adapted surface highlights. Here, we want to figure out the usefulness as well as the applicability to examine the flow in the medical and biomedical research stage.

7.1. Evaluation of surface shading

We performed an informal evaluation for the three shading techniques: semitransparency (ST_1), fresnel opacity (ST_2) according to Gasteiger *et al.* [GNKP10] and our shading (ST_3) based on the suggestive contour measure, see Figure 6. The goal was to assess their capabilities for expressing relevant surface characteristics while simultaneously provide appropriate visibility of the embedded streamline visualization. We wanted to figure out which of the proposed shading techniques yields the most expressive results. Therefore, we conducted an evaluation with one physician, two CFD engineers involved in hemodynamic analysis and six researchers with background in medical visualization. We chose four representative vessel structures consisting of three cerebral aneurysms and one aorta data set. During the evaluation, we noted the participants' spoken comments and the participants were able to adjust the parameter settings for each technique, i.e. transparency value for ST_1 , edge fall-off parameter for ST_2 and brightness value c for ST_3 .

(recall Section 5.4). For each data set and technique, the participants were asked to perform three tasks:

1. Identification of salient surface features such as concave, convex regions and performance assessment of each shading technique to accomplish the task.
2. Visibility assessment of the embedded streamlines.
3. Assessment of spatial relationship and depth perception between vessel sections.

For *task 1*, technique ST_3 was rated as most efficient and it revealed more surface features compared to ST_1 and ST_2 . The participants stated that certain curvature features at branches and bulges on the aneurysm sac were more clearly depicted with ST_3 than with ST_1 and ST_2 (see Figure 6, third row). An increase of the opacity for ST_1 improved the perception, but also increased the occlusion of the embedded streamlines. Therefore, technique ST_2 was rated better than ST_1 because an increased edge fall-off reveals more shape features but still ensures visibility of the flow facing towards the viewer. Most of the participants also appreciated the capability of ST_3 to convey the salient surface features even in still images. For some vessel structures, the other two techniques required more camera interaction efforts to obtain an overview about the shape.

The assessment in *task 2* was rated most efficient for technique ST_3 when using a brightness value around 1.5. Larger values would occlude more streamlines, which is similar to ST_2 in terms of the edge fall-off value (in average 1.5). For this technique, some participants criticized the increased occlusion of surface parts facing away from the viewer. As expected for ST_1 , an increased transparency improves also the streamline visibility but decreases the shape depiction. Some participants stated that this assessment depends on the exploration task, i.e. focusing on embedded flow or on flow and enclosing vessel.

For *task 3*, ST_2 and ST_3 were rated as most efficient compared to ST_1 because of the added shadow and depth cues. Thereby, blurring and depth attenuation were evaluated equally expressive with slightly more preference for blurring because of its more natural adaption to the human depth perception. Two participants also asked for a possibility to change the region of interest for the focus region by clicking on a specific vessel section.

7.2. Informal feedback on nearby-pathline surface highlighting

We performed an informal interview with a domain expert to gain a qualitative user feedback. The expert is actively involved in the exploration of hemodynamics in cerebral aneurysms. The interview was designed to determine if the animation is useful and supports the expert in his diagnostic activities, such as the identification of slow and fast flow regions as well as near-wall flow. Therefore, we showed him four different data sets, see Figure 7. The domain expert was asked to examine different aneurysms with pathline animation. It was first stated that it is useful to illustrate the pathlines over the whole time with desaturated colour-coded information, e.g. flow speed and vorticity. The animations are visually pleasant and the exploration with step back and step forward is helpful. Furthermore, the expert explained that the examination of near-wall hemodynamics is of high importance since it can be an indicator for

aneurysm rupture in the past and the increased risk for rupture. Thus, the highlighting is appropriate to assess the pathline distances to the surface. Here, less camera rotation is needed to estimate distances. The interruption if the animation during camera rotation, was also stated to be very efficient to analyse specific regions. In summary, the domain expert was satisfied with the pathline animation and with the highlighting of nearby surface regions. Furthermore, the domain expert suggested to integrate different options for future work. For example, it would be useful to depict other information during the animation such as WSS. As the domain expert liked the surface shading, another suggestion is to decode the distances with another colour bar. This would enhance the distance estimation.

8. Conclusion and Future Work

In this paper, we have presented a novel adaptive surface visualization technique for blood vessels with embedded flow information. The shading technique is based on the *suggestive contour* measure, which ensures both an appropriate depiction of relevant local surface features and the visibility of the embedded flow visualization. Furthermore, we incorporate depth blurring to enhance the perception of depth and spatial relationships. Our informal evaluation with domain experts demonstrated an improved shape perception compared to existing techniques while simultaneously ensuring appropriate visibility of the embedded flow visualization. Moreover, our approach is able to convey the salient surface features in still images, which also enables its utilization for documentation purposes. Besides its application on vessels with embedded flow information, our approach is also applicable to other non-vessel surfaces such as liver surfaces with internal structures and bone structures, as shown in Figure 8.

For future work, we consider a controlled user study to quantify the performance of our approach compared to a semi-transparent vessel visualization and the ghosted view approach by Gasteiger *et al.* [GNKP10]. This study is inspired by Baer *et al.* [BGCP11] and includes task-driven experiments such as adjusting of surface normals or distance estimations of vessel sections. The quantitative performance of each shading technique can be assessed based on the accuracy and response time of each task. Furthermore, we would like to use different colour bars to decode the distances of pathline-nearby surface regions. This colour-coding would improve the assessment of the distances of the pathlines to the vessel surface. Moreover, we would like to improve the distance calculation based on spatial data structures as described in Zhou *et al.* [ZHGW08]. They incorporate the k-d tree calculation on the GPU and their method would significantly improve the calculation time.

Acknowledgements

The authors would like to thank Uta Preim (Hospital Magdeburg, Germany), Daniel Stucht (Institute of Biomedical Magnetic Resonance, University Magdeburg, Germany), Philipp Berg (Institute of Fluid Mechanics and Thermodynamics, University Magdeburg, Germany) and Mathias Neugebauer (Institute for Simulation and Graphics, University Magdeburg, Germany) for their valuable feedback in the evaluations. Furthermore, we thank Fraunhofer MEVIS Bremen, Germany, for providing the prototyping platform MeVisLab.

References

- [AML*08] APPANABOYINA S., MUT F., LÖHNER R., PUTMAN C., CEBRAL J.: Computational fluid dynamics of stented intracranial aneurysms using adaptive embedded unstructured grids. *Numerical Methods in Fluids* 57, 5 (2008), 475–493.
- [Ben75] BENTLEY J. L.: Multidimensional binary search trees used for associative searching. *Communications ACM* 18, 9 (Sept. 1975), 509–517.
- [BGCP11] BAER A., GASTEIGER R., CUNNINGHAM D. W., PREIM B.: Perceptual evaluation of ghosted view techniques for the exploration of vascular structures and embedded flow. *Computer Graphics Forum* 30, 3 (2011), 811–820.
- [BKP*10] BOTSCH M., KOBELT L., PAULY M., ALLIEZ P., UNO LEVY B.: *Polygon Mesh Processing*. AK Peters, Natick, MA, USA, 2010.
- [BMGS13] BORN S., MARKL M., GUTBERLET M., SCHEUERMANN G.: Illustrative visualization of cardiac and aortic blood flow from 4D MRI data. In *Proceedings of the IEEE Pacific Visualization* (2013), pp. 129–136.
- [BSH*10] BAHAROGLU M. I., SCHIRMER C. M., HOIT D. A., GAO B.-L., MALEK A. M.: Aneurysm inflow-angle as a discriminant for rupture in sidewall cerebral aneurysms morphometric and computational fluid dynamic analysis. *Stroke* 41, 7 (2010), 1423–1430.
- [BWF*10] BORN S., WIEBEL A., FRIEDRICH J., SCHEUERMANN G., BARTZ D.: Illustrative stream surfaces. *IEEE Transaction on Visualization and Computer Graphics* 16, 6 (2010), 1329–1338.
- [CCA*05] CEBRAL J. R., CASTRO M. A., APPANABOYINA S., PUTMAN C. M., MILLAN D., FRANGI A. F.: Efficient pipeline for image-based patient-specific analysis of cerebral aneurysm hemodynamics: Technique and sensitivity. *IEEE Transaction Medical Imaging* 24, 4 (2005), 457–467.
- [CMWP11] CEBRAL J. R., MUT F., WEIR J., PUTMAN C. M.: Association of hemodynamic characteristics and cerebral aneurysm rupture. *American Journal of Neuroradiology* 32, 2 (2011), 264–270.
- [DFRS03] DECARLO D., FINKELSTEIN A., RUSINKIEWICZ S., SANTELLA A.: Suggestive contours for conveying shape. In *Proceedings of ACM SIGGRAPH* (2003), pp. 848–855.
- [DWE03] DIEPSTRATEN J., WEISKOPF D., ERTL T.: Interactive cutaway illustrations. *Computer Graphics Forum* 22, 3 (2003), 523–532.
- [EBR*11] EVERTS M. H., BEKKER H., ROERDINK JOS B. T. M., ISENBERG T.: Illustrative line styles for flow visualization. In *Proceedings of the IEEE Pacific Graphics* (2011), pp. 105–110. Short paper.
- [GGSC98] GOOCH A., GOOCH B., SHIRLEY P., COHEN E.: A non-photorealistic lighting model for automatic technical illustration. In *Proceedings of the ACM SIGGRAPH* (1998), pp. 447–452.
- [GNBP11] GASTEIGER R., NEUGEBAUER M., BEUNG O., PREIM B.: The FlowLens: A focus-and-context visualization approach for exploration of blood flow in cerebral aneurysms. *IEEE Transaction on Visualization and Computer Graphics* 17, 12 (2011), 2183–2192.
- [GNKP10] GASTEIGER R., NEUGEBAUER M., KUBISCH C., PREIM B.: Adapted surface visualization of cerebral aneurysms with embedded blood flow information. In *Proceedings of the EG Workshop on Visual Computing for Biology and Medicine* (2010), pp. 25–32.
- [HFS*11] HENNEMUTH A., FRIMAN O., SCHUMANN C., BOCK J., DREXL J., MARKL M., PEITGEN H.-O.: Fast interactive exploration of 4D MRI flow data. In *Proceedings of the SPIE Medical Imaging* (2011), vol. 7964, pp. 79640E:1–79640E:11.
- [HGH*10] HUMMEL M., GARTH C., HAMANN B., HAGEN H., JOY K. I.: Iris: Illustrative rendering for integral surfaces. *IEEE Transaction on Visualization and Computer Graphics* 16, 6 (2010), 1319–1328.
- [IFH*03] ISENBERG T., FREUDENBERG B., HALPER N., SCHLECHTWEG S., STROTHOTTE T.: A developer's guide to silhouette algorithms for polygonal models. *IEEE Transaction on Computer Graphics and Applications* 23, 4 (2003), 28–37.
- [IFP95] INTERRANTE V., FUCHS H., PIZER S.: Enhancing transparent skin surfaces with ridge and valley lines. In *Proceedings of the IEEE Visualization* (1995), pp. 52–59.
- [IFP97] INTERRANTE V., FUCHS H., PIZER S. M.: Conveying the 3D shape of smoothly curving transparent surfaces via texture. *IEEE Transactions on Visualization and Computer Graphics* 3, 2 (1997), 98–117.
- [JDA07] JUDD T., DURAND F., ADELSON E.: Apparent ridges for line drawing. In *Proceedings of the ACM SIGGRAPH* (2007), p. 19.
- [Juv11] JUVELA S.: Prevalence of and risk factors for intracranial aneurysms. *The Lancet Neurology* 10, 7 (2011), 595–597.
- [KBDL09] KARMONIK C., BISMUTH J., DAVIES M., LUMSDEN A.: Computational fluid dynamics as a tool for visualizing hemodynamic flow patterns. *Methodist DeBakey Cardiovascular Journal* 5, 3 (2009), 26–33.
- [KGP*13] KÖHLER B., GASTEIGER R., PREIM U., THEISEL H., GUTBERLET M., PREIM B.: Semi-automatic vortex extraction in 4D PC-MRI cardiac blood flow data using line predicates. *IEEE Transaction on Visualization and Computer Graphics* 19(12) (2013), 2773–2782.
- [KHSI04] KIM S., HAGH-SHENAS H., INTERRANTE V.: Conveying shape with texture: Experimental investigations of texture's effects on shape categorization judgments. *IEEE Transaction on Visualization and Computer Graphics* 10, 4 (2004), 471–483.
- [LABFL09] LESAGE D., ANGELINI E. D., BLOCH I., FUNKA-LEA G.: A review of 3D vessel lumen segmentation techniques: Models,

- features and extraction schemes. *Medical Image Analysis* 13, 6 (2009), 819–845.
- [LCD06] LUFT T., COLDITZ C., DEUSSEN O.: Image enhancement by unsharp masking the depth buffer. *ACM Transaction on Graphics* 25 (2006), 1206–1213.
- [LGP13a] LAWONN K., GASTEIGER R., PREIM B.: Adaptive surface visualization of vessels with embedded blood flow based on the suggestive contour measure. In *Proceedings of the International Workshop on Vision, Modeling and Visualization* (Lugano, Switzerland, 2013), M. M. Bronstein, J. Favre and K. Hormann (Eds.), pp. 113–120.
- [LGP13b] LAWONN K., GASTEIGER R., PREIM B.: Qualitative evaluation of feature lines on anatomical surfaces. In *Proceedings of Bildverarbeitung für die Medizin* (2013), pp. 187–192.
- [LHZP07] LARAMEE R., HAUSER H., ZHAO L., POST F.: Topology-Based Flow Visualization, The State of the Art. In *Topology-based Methods in Visualization*, H. Hauser, H. Hagen and H. Theisel (Eds.), Mathematics and Visualization. Springer, Berlin, Heidelberg (2007), pp. 1–19.
- [MDSB02] MEYER M., DESBRUN M., SCHRÖDER P., BARR A. H.: Discrete differential-geometry operators for triangulated 2-manifolds. In *Proceedings of the VisMath* (2002), pp. 35–57.
- [MFK*12] MARKL M., FRYDRYCHOWICZ A., KOZERKE S., HOPE M., WIEBEN O.: 4D flow MRI. *Journal of Magnetic Resonance Imaging* 36, 5 (2012), 1015–1036.
- [MLP*10] MCLOUGHLIN T., LARAMEE R. S., PEIKERT R., POST F. H., CHEN M.: Over two decades of integration-based, geometric flow visualization. *Computer Graphics Forum* 29, 6 (2010), 1807–1829.
- [MNP11] MÖNCH T., NEUGEBAUER M., PREIM B.: Optimization of vascular surface models for computational fluid dynamics and rapid prototyping. In *Proceedings of the Second International Workshop on Digital Engineering* (2011), pp. 16–23.
- [MTHG03] MATTAUSCH O., THEUSSL T., HAUSER H., GRÖLLER E.: Strategies for interactive exploration of 3D flow using evenly-spaced illuminated streamlines. In *Proceedings of the ACM Spring Conference on Computer Graphics* (2003), pp. 230–241.
- [NLB*13] NEUGEBAUER M., LAWONN K., BERG P., JANIGA G., BEUNG O., PREIM B.: AmniVis - A system for qualitative exploration of near-wall hemodynamics in cerebral aneurysms. *Computer Graphics Forum* 32, 3pt3 (2013), 251–260.
- [PB13] PREIM B., BOTHA C.: *Visual Computing for Medicine*. 2nd edition, Morgan Kaufmann, Burlington, MA, USA, 2013.
- [Pel12] PELT R. F. P. V.: *Real-time Illustrative Visualization of Cardiovascular Hemodynamics*. PhD thesis, Technical University of Eindhoven, 2012.
- [RBD06] RUSINKIEWICZ S., BURNS M., DECARLO D.: Exaggerated shading for depicting shape and detail. In *Proceedings of the ACM SIGGRAPH* 25, 3 (2006), pp. 1199–1205.
- [RHD*06] RITTER F., HANSEN C., DICKEN V., KONRAD O., PREIM B., PEITGEN H.-O.: Real-time illustration of vascular structures. *IEEE Transaction on Visualization and Computer Graphics* 12, 5 (2006), 877–884.
- [SABS94] SALISBURY M. P., ANDERSON S. E., BARZEL R., SALESIN D. H.: Interactive pen-and-ink illustration. In *Proceedings of the 21st annual conference on Computer graphics and interactive techniques, ACM SIGGRAPH* (New York, NY, USA, 1994), ACM, pp. 101–108.
- [Sch97] SCHÖBERL J.: NETGEN: An advancing front 2D/3D-mesh generator based on abstract rules. *Computing and Visualization in Science* 1 (1997), 41–52.
- [SEA09] SVAKHINE N. A., EBERT D. S., ANDREWS W. M.: Illustration-inspired depth enhanced volumetric medical visualization. *IEEE Transaction on Visualization and Computer Graphics* 15, 1 (2009), 77–86.
- [SJWS08] SALZBRUNN T., JÄNICKE H., WISCHGOLL T., SCHEUERMANN G.: The state of the art in flow visualization: Partition-based techniques. In *Proceedings of the Simulation and Visualization* (2008), pp. 75–92.
- [TGE97] TEITZEL C., GROSSO R., ERTL T.: Efficient and reliable integration methods for particle tracing in unsteady flows on discrete meshes. In *Proceedings of the Visualization in Scientific Computing* (1997), pp. 31–41.
- [TPB*08] TIETJEN C., PFISTERER R., BAER A., GASTEIGER R., PREIM B.: Hardware-accelerated illustrative medical surface visualization with extended shading maps. In *Proceedings of SmartGraphics* (2008), pp. 166–177.
- [Vio05] VIOLA I.: *Importance-Driven Expressive Visualization*. PhD thesis, Institute of Computer Graphics and Algorithms, Vienna University of Technology, June 2005.
- [VPvP*12] VILANOVA A., PREIM B., VAN PELT R., GASTEIGER R., NEUGEBAUER M., WISCHGOLL T.: Visual exploration of simulated and measured blood flow. *CoRR abs/1209.0999* (2012).
- [WFG92] WANGER L. R., FERWERDA J., GREENBERG D. P.: Perceiving spatial relationships in computer-generated images. *IEEE Transaction on Computer Graphics and Applications* 12, 3 (1992), 44–58.
- [XHT*07] XIE X., HE Y., TIAN F., SEAH H.-S., GU X., QIN H.: An effective illustrative visualization framework based on photic extremum lines. *IEEE Transaction on Visualization and Computer Graphics* 13 (2007), 1328–1335.
- [ZHWG08] ZHOU K., HOU Q., WANG R., GUO B.: Real-time KD-tree construction on graphics hardware. In *Proceedings of the ACM SIGGRAPH Asia* (2008), ACM, pp. 126:1–126:11.